On the Characterization of VBR MPEG Streams*

Marwan Krunz
Department of ECE
University of Arizona
Tucson, AZ 85721
krunz@ece.arizona.edu

Satish K. Tripathi
Department of CS
University of Maryland
College Park, MD 20742
tripathi@cs.umd.edu

Abstract

We present a comprehensive model for variable-bit-rate MPEG video streams. This model captures the bit-rate variations at multiple time scales. Long-term variations are captured by incorporating scene changes, which are most noticeable in the fluctuations of I frames. The size of an I frame is modeled by the sum of two random components: a scene-related component and an AR(2) component that accounts for the fluctuations within a scene. Two random processes of *i.i.d.* rvs are used to model the sizes of P and B frames, respectively. The complete model is then obtained by intermixing the three sub-models according to a given GOP pattern. It is shown that the composite model exhibits long-range dependence (LRD) in the sense that its autocorrelation function is non-summable. The LRD behavior is caused by the repetitive GOP pattern which induces periodic cross-correlations between different types of frames. Using standard statistical methods, we successfully fit our model to several empirical video traces. We then study the queueing performance for video traffic at a statistical multiplexer. The results show that the model is sufficiently accurate in predicting the queueing performance for real video streams.

1 Introduction

A BISDN/ATM network will transport a variety of streams with different traffic patterns and performance requirements. Accurate characterization of these streams is essential to dimensioning network resources and providing acceptable levels of quality of service.

In this paper, we investigate the modeling of MPEG-coded video movies. The literature contains many studies on the modeling of variable bit rate (VBR) video based on different compression techniques. Following the standardization of the MPEG algorithm and its wide acceptance, researchers started investigating the characteristics of MPEG-coded video traffic and developing source models specific to this type of traffic [6, 9, 18, 19, 16, 8, 17]. At first, the focus was on MPEG streams without interpolative (B) frames [9, 19, 16], whose encoding and decoding delay makes them unattractive for real-time video. In [8] Huang et al. proposed a self-similar fractal model for MPEG video, which captures the correlation structure and frame-size distribution for the three types of MPEG frames. While matching both statistics warrants a good approximation of the second-order properties, it does not capture the multiple-time-scale variations observed in real traces. Heyman et al. [6] attempted to provide appropriate fittings for the size of each type of MPEG frames, and concluded that more work is still needed to model P and B frames.

Our work is being motivated by the need for a comprehensive characterization of MPEG-coded video streams that explicitly incorporates the multiple-time-scale variations of the bit rate. The proposed model can be used to generate synthetic MPEG streams for network performance studies and resource allocation at video servers. Generating synthetic streams has two obvious advantages. First, performance studies can be carried out without requiring the actual traces (which may not be available). Second, a stochastic model encompasses many realizations which represent "structurally" similar but not identical synthetic streams. These synthetic realizations are ideal for statistical multiplexing studies (a single empirical trace is hardly appropriate for generating multiple streams that have the same stochastic structure, but are not identical). Our model is comprehensive in the sense that it characterizes an MPEG stream with I, P, and B frames. In addition to approximating the marginal distribution and autocorrelation structure of the empirical data, the model captures the impact of scene changes on the bit rate variations.

The idea of incorporating scene changes in a traffic model is not particularly new. In the DAR(1) model [10], frame sizes are generated according to a finite-state Markov chain, where each state corresponds to a given frame size. Once the chain enters a state, it stays there for an exponentially distributed time, which can be associated with a scene duration. Video frames within a scene have the same size. Frater et al. [4] enhanced the DAR(1) model by using a different distribution for scene durations which resulted in better predictions of the queueing performance. However, similar to the DAR(1) model, the "scenic" model of Frater does not incorporate the bit-rate variations within scenes. Moreover, both models were developed for JPEG-like streams (i.e., MPEG streams with I frames only), whose empirical autocorrelation function decreases almost monotonically. Scene effects were also incorporated in [15] for the modeling of JPEG-like VBR video based on the TES approach. For MPEG streams with I, P, and B frames, the empirical

* This research was supported by NSF grant # 9318933 and by a Shared University Research IBM grant.

To appear in the Proceedings of ACM SIGMETRICS'97 Conference, May 1997, Seatle, Washington.

autocorrelation function has a complicated structure with multiple pseudo-periodic components. In [12], we examined the empirical statistics for I, P, and B frames. The present work is a continuation of our effort to provide a complete source model for MPEG traffic.

The paper in structured as follows. In Section 2 we briefly describe the empirical traces used in this study. In Section 3 we present the source model. Section 4 provides an algorithm for generating synthetic streams. Trace-driven simulations using both real and synthetic streams are conducted in Section 5. The paper is concluded in Section 6.

2 Empirical MPEG Sequences

Table 1 depicts the four public domain traces which are used in our study. Each trace represents the sizes of the compressed frames in an MPEG-coded video movie (see references for compression details). The rationale for using several traces is to demonstrate the applicability of the model to videos with diverse content. For brevity, we describe the fitting procedure with reference to one trace and summarize the fitting outcome for the four traces.

Trace	Frames	(N, M)
Wizard of Oz (Oz) [12]	41760	$(15, 3)$
Star Wars [5]	174066	$(12, 3)$
Silence of the Lambs [18]	40000	$(12, 3)$
Goldfinger [18]	40000	$(12, 3)$

Table 1: Empirical video traces (from MPEG-1 encoders).

Standard MPEG encoders generate three types of compressed frames: I, P, and B. While I frames are intra-coded, the generation of P and B frames involve, in addition to intra-coding, the use of motion prediction and interpolation techniques. As a result, I frames are, on average, the largest in size, followed by P frames, and finally B frames. A representative sample of a VBR sequence is shown in Figure 1.

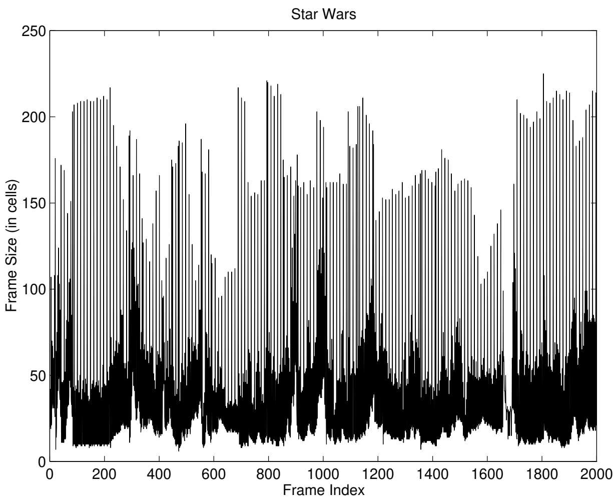

Figure 1: Representative sample of the frame-size sequence.

An important feature of common MPEG encoders (both hardware and software) is the manner in which frame types are generated. Although not required by the standards, typical encoders use a fixed Group-of-Pictures (GOP) pattern when compressing a video sequence (the GOP pattern specifies the number and temporal order of P and B frames between two successive I frames). Quite often the fixed GOP pattern is "regular" in the sense that the number of B frames between two reference frames (I or P) is fixed. Such a GOP pattern can be characterized by two parameters: the I-to-I frame distance (N), and the I-to-P frame distance (M) (if no P frames are used, then $M = N$). We limit our treatment to "regular" GOP patterns. It should be emphasized that MPEG-compliant sequences *need not* use a "regular" GOP pattern, and not even a repetitive one. However, since many sequences are being coded with regular GOP patterns (often to simplify the codec design), developing a traffic model for such sequences has its merits.

Due to the non-causal nature of motion interpolation in the coding of B frames, a sequence of compressed frames is usually rearranged before transmission over the network according to the frames' decoding order. However, and with the exception of the first few frames, both temporal and transmission orders of an MPEG sequence exhibit the same periodic behavior of the GOP pattern (although the dependency structure is now different), as is exemplified in Figure 2. Thus, the impact of a repetitive GOP pattern will also be reflected inside the network, and must be considered when modeling network traffic.

The autocorrelation function (ACF) for *Oz* trace is shown in Figure 3. Its structure is strongly influenced by the form of the GOP pattern. Two apparent periodic components are observed in the ACF: one at lags of kN and the other at lags of kM, where $k = 0, 1, 2, \ldots$. Both components decay very slowly; an early indication of LRD.

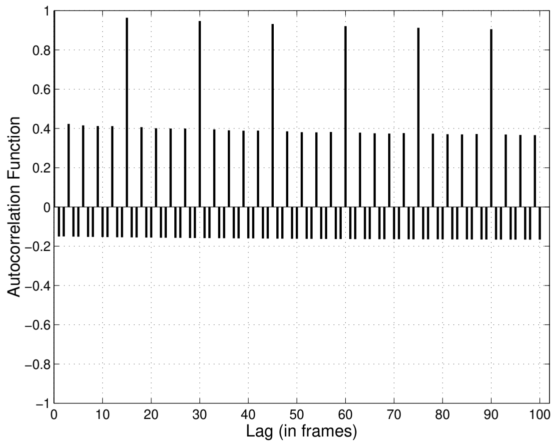

Figure 3: ACF of an MPEG-coded stream (*Oz* trace).

3 Modeling a VBR MPEG Stream

3.1 Scene Length Distribution

It is observed from Figure 1 that I frames exhibit different VBR dynamics at different time scales. At a time scale of the order of few seconds, the bit rate fluctuates in small amounts about some mean level, which itself varies drastically at a larger time scale. The fluctuations in the mean levels at the larger time scale are often attributed to "scene" changes [15, 4, 7]. A scene, in the visual sense, is loosely defined as a portion of the movie without sudden changes in view, but with some panning and zooming [15]. Incorporating a "scenic" component in a traffic model gives the VBR

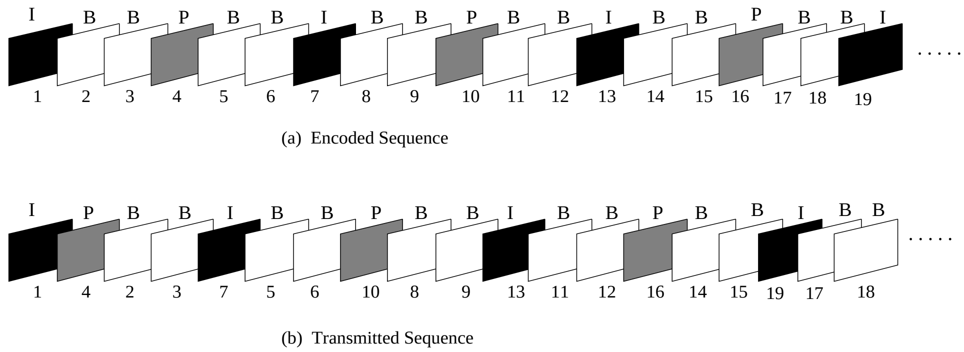

Figure 2: Encoding and transmission orders of an MPEG sequence.

dynamics a physical interpretation and often leads to better performance predictions. In [11] we introduced a heuristic method to determine scene boundaries using only the sizes of I frames. This heuristic is based on the premise that "significant" changes in the sizes of consecutive I frames are strong indications of scene changes. We use this heuristic to obtain the sequence of scene lengths for each trace. Note that scene lengths are computed to an accuracy of a GOP period (i.e., 30 seconds). This has minor impact on the goodness of the fit since a scene lasts on average for several seconds. Figure 4 shows an example of the I frame subsequence (from *Star Wars* trace) and the corresponding computed scenes.

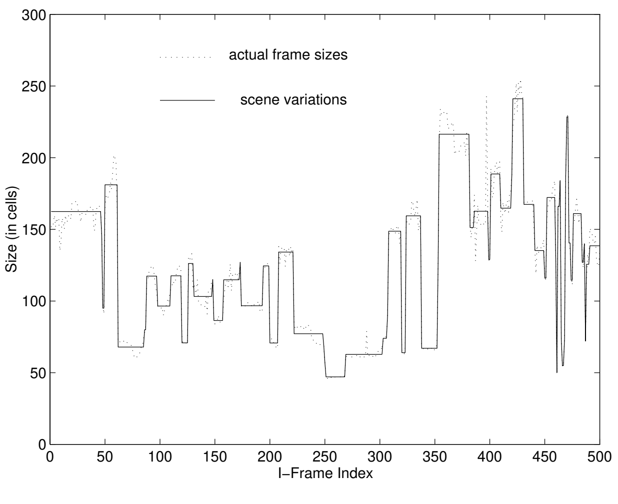

Figure 4: Fluctuations of I frames and the computed scenes.

Summary statistics of the computed scene lengths for the four traces are given in Table 2. The average scene length can be used as a one-parameter indication of the overall level of activity of a movie (the higher the action of the movie, the smaller the average scene length).

Several studies have indicated that the scene length distribution can be appropriately fitted by an exponential (or geometric) distribution [10, 15]. Although we use a different approach to compute scene lengths, we also found the geometric fit to be appropriate for our data (except for some deviation in the extreme tail of the distribution which cannot be accurately fitted due to the small number of scenes with long durations). Accordingly, we model the scene length by a geometrically distributed rv with parameter q ($q < 1$). Let N_j be the length of the jth scene ($j = 1, 2, \ldots$). Then, $\Pr\{N_j = n\} = q^{n-1}(1-q)$, for $n = 1, 2, \ldots$. The mean scene length is $E[N_j] = 1/(1-q)$. We tested the hypothesis of independence of scene lengths using the runs-up test [14] and found that at a 95% level of confidence, this hypothesis cannot be rejected. Hence, we assume that $\{N_j\}$ are *i.i.d.* with common geometric distribution.

3.2 Frame Size Distributions

Two important factors determine the size of an MPEG frame: the scene activity and the frame type. The effect of the scene activity occurs at a time scale of few seconds (the average scene length). Frame types are determined by the GOP pattern, so their impact is observed at a smaller time scale (e.g., 1/30 sec). To capture the impact of the frame type, we use a composite model which consists of three random processes. Each process generates the sizes of one type of frames. The three processes are intermixed according to a given GOP pattern to produce the overall frame size sequence. As shown later, the periodic nature of the GOP pattern induces strong cross-correlations between frames of different types.

While scene dynamics affect the sizes of the three types of frames, the impact is particularly noticeable (and thus easier to capture) in the case of I frames. This is due to the fact that I frames are only intra-coding, so less factors influence their sizes. Accordingly, we incorporate a scene-related component in the modeling of I frames, and ignore scene effects in P and B frames. This simplifying assumption should not have a critical impact on the cell loss probability or on other performance measures that are mainly affected by large frames (which are typically I frames).

3.2.1 I Frames

As noted earlier, the sizes of I frames *within* a scene fluctuate slightly around an average level that corresponds to the mean activity of the scene. Let $X_I(n)$ be the size of the nth I frame. We model $X_I(n)$ by the sum of two independent random variables:

$$X_I(n) = X_I^*(n) + \Delta_I(n) \tag{1}$$

where $X_I^*(n)$ represents the mean activity of the scene and $\Delta_I(n)$ represents the fluctuation of the nth I frame about $X_I^*(n)$. First, consider $X_I^*(n)$. This quantity is constant for all I frames in the same scene, and it varies from one scene to another. For the jth scene that starts with the kth I

Trace	Number of Computed Scenes	Scene Length Statistic (in consecutive I frames)			
		Mean	Std. Deviation	Max.	Min.
Oz	199	14.0 (7 sec)	17.3	90	1
Star Wars	2452	5.92 (2.96 sec)	7.85	78	1
Silence of the Lambs	327	10.2 (5.1 sec)	18.1	209	1
Goldfinger	441	7.6 (3.8 sec)	9.4	66	1

Table 2: Summary statistics of the computed scene lengths.

frame, we have

$$X_I^*(k) = X_I^*(k+1) = \cdots = X_I^*(k+N_j-1) \stackrel{\triangle}{=} \widetilde{X}_I(j) \quad (2)$$

We assume $\{\widetilde{X}_I(j) : j = 1, 2, \ldots\}$ are *i.i.d.* with common *pdf* $f_{\widetilde{X}_I}$. This assumption is justified by the weak presence of correlations in the empirical sequence $\{\widetilde{X}_{I,emp}(j)\}$, where $\widetilde{X}_{I,emp}(j)$ is the sample average of the sizes of I frames in the jth scene of an empirical trace. In [12] we examined three fits for the distribution of $\widetilde{X}_I$: Gamma, Weibull, and lognormal. We found the lognormal fit to be the most appropriate. Accordingly, we let $\widetilde{X}_I(j) \sim$ lognormally distributed with parameters $\widetilde{\mu}_I$ and $\widetilde{\sigma}_I$:

$$f_{\widetilde{X}_I}(u) = \begin{cases} \frac{1}{u\sqrt{2\pi\widetilde{\sigma}_I^2}} \exp\left[\frac{-(\ln u - \widetilde{\mu}_I)^2}{2\widetilde{\sigma}_I^2}\right], & u > 0 \\ 0, & otherwise \end{cases} \quad (3)$$

The mean ($m_{\widetilde{X}_I}$) and the variance ($v_{\widetilde{X}_I}$) of $\widetilde{X}_I$ are given by:

$$m_{\widetilde{X}_I} = \exp\left\{\widetilde{\mu}_I + \widetilde{\sigma}_I^2/2\right\} \quad (4)$$

$$v_{\widetilde{X}_I} = \exp\left\{2\widetilde{\mu}_I + \widetilde{\sigma}_I^2\right\}\left(\exp\left\{\widetilde{\sigma}_I^2\right\} - 1\right) \quad (5)$$

$\widetilde{\mu}_I$ and $\widetilde{\sigma}_I$ are estimated by their Maximum Likelihood Estimates (MLE) (see Table 4).

Proposition 1 *Let $f^{(n)}_{X_I^*}$ be the pdf for $X_I^*(n)$. Then*

$$f^{(n)}_{X_I^*} = f_{\widetilde{X}_I}, \text{ for all } n, \quad (6)$$

i.e., $\{X_I^*(n)\}$ is a (correlated) identically distributed random sequence.

Proof: (by induction). It is clear that $f^{(1)}_{X_I^*} = f_{\widetilde{X}_I}$. Suppose that $f^{(n)}_{X_I^*} = f_{\widetilde{X}_I}$. The probability that the nth and the $(n+1)$th I frames are in the same scene is q. In this case, $X_I^*(n) = X_I^*(n+1)$, which implies that the two random variables are equal in distribution. With probability $1-q$, the $(n+1)$th I frame is the starting frame of a new scene, in which case $f^{(n+1)}_{X_I^*} = f_{\widetilde{X}_I}$ which is also equal to $f^{(n)}_{X_I^*}$. Thus, $f^{(n)}_{X_I^*} = f^{(n+1)}_{X_I^*}$. By induction on n, the assertion is true. □

Next, consider $\Delta_I(n)$. For a given trace, we compute the empirical sequence $\{\widehat{\Delta}_I(n)\}$, where $\widehat{\Delta}_I(n) = X_{I,emp}(n) - \widetilde{X}_{I,emp}(j_n)$, j_n being the scene index to which the nth I frame belongs. The sequence $\{\widehat{\Delta}_I(n)\}$ is then fitted by the stochastic process $\{\Delta_I(n)\}$. Notice that $\{\Delta_I(n)\}$ is independent of $\{X_I^*(n)\}$, and thus invariant to scene changes. The sample ACF for $\{\widehat{\Delta}_I(n)\}$ in *Oz* trace is shown in Figure 6. Its fast decay suggests considering an autoregressive (AR) model for $\{\Delta_I(n)\}$. The order of the AR fit is determined based on the *partial autocorrelation function* (PACF) [2] for $\{\widehat{\Delta}_I(n)\}$, which is shown in Figure 6. The PACF clearly indicates non-negligible first and second autoregressive coefficients, suggesting an AR(2) fit. Accordingly, we characterize $\{\Delta_I(n)\}$ by an AR(2) process:

$$\Delta_I(n) = a_1\Delta_I(n-1) + a_2\Delta_I(n-2) + \varepsilon(n) \quad (7)$$

where $\{\varepsilon(n)\}$ is a sequence of *i.i.d.* random variables with mean zero and variance σ_ε^2. To determine an appropriate distribution for the residuals, let f_ε and f_Δ be the *pdf* for $\varepsilon(n)$ and $\Delta_I(n)$, respectively. The shape of f_Δ can be inferred from the histogram of $\{\widehat{\Delta}_I(n)\}$, which is shown in Figure 7 for *Oz* trace (similar results are obtained for the other traces). A normal fit is adequate. Hence, we let $f_\Delta = N(0, \sigma_\Delta^2)$. A normal distribution for $\{\Delta_I(n)\}$ arises naturally when the residuals are also normally distributed. Hence, we let $f_\varepsilon = N(0, \sigma_\varepsilon^2)$.

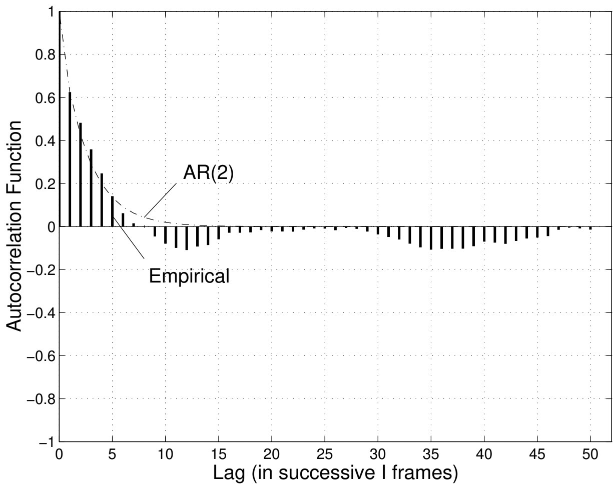

Figure 5: Autocorrelations in $\{\widehat{\Delta}_I(n)\}$ (*Oz* trace).

At this point, it is instructive to briefly compare our model for I frames with other previously proposed models. In [7] an AR(2) model was suggested for a video-teleconferencing stream generated from an H.261-compliant encoder. Videoconferencing exhibits less scene dynamics than movies, thus only the AR(2) component is needed. Similar to our model, a video sequence in the DAR(1) model [10] consists of several scenes with exponentially distributed *i.i.d.* durations. A negative binomial distribution, and later a discretized lognormal distribution [6], was suggested for the average frame size in the DAR(1) model. Fluctuations within a scene are not incorporated. The "scenic" model of Frater et al. [4] is similar to the DAR(1) model except for scene durations which have a *pdf* of the form $p(x) = a/(x^n + b^2)$ ($n \approx 2$ for *Star Wars*). While such a *pdf* provided better approximation of the empirical ACF in *Star Wars* trace, it can

Feature	Ours	DAR(1)	Frater et al. model [4]	Video-teleconferencing model [7]
Compression	MPEG	H.261 and JPEG	JPEG	H.261
Scene durations	geometric	exponential	$a/(x^n + b^2)$	—
Intra-scene variations	AR(2)	—	—	AR(2)

Table 3: Scene-based time series models for I frames.

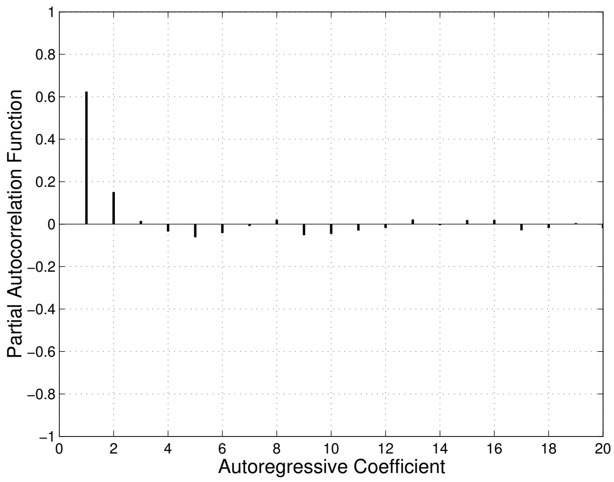

Figure 6: Partial autocorrelations in $\{\widehat{\Delta}_I(n)\}$ (Oz trace).

be shown that this choice renders the model nonstationary. Variations within scenes were not accounted for in the "scenic" model. Our belief is that detailed characterization of scene durations is important when considering a sequence of I frames only. When I frames are intermixed with P and B frames, the significant differences between the sizes of different types of frames along with the periodicity of the GOP pattern are the major factors that impact the correlation structure. Our model for I frames can be regarded as a generalization of both the AR(2) model for video-teleconferencing and the DAR(1) model. Table 3 summarizes the scene-related differences between our model and other similar models.

Estimates of a_1 and a_2 in (7) can be obtained using Yule-Walker equations [2]:

$$\begin{bmatrix} a_1 \\ a_2 \end{bmatrix} = \begin{bmatrix} 1 & r_1 \\ r_1 & 1 \end{bmatrix}^{-1} \begin{bmatrix} r_1 \\ r_2 \end{bmatrix} \tag{8}$$

where r_k is the sample ACF for $\{\widehat{\Delta}_I(n)\}$ at lag k. Using these estimates, the sequence $\{\widehat{\Delta}_I(n)\}$ is fitted to an AR(2) model. The ACF of the experimental residuals is shown in Figure 8. The absence of correlations among the residuals is a strong evidence of the appropriateness of the model. An estimate of σ_ε^2 is given by the the sum-of-squares of the experimental residuals divided by the number of I frames. The variance of $\Delta_I(n)$ is given by:

$$\sigma_\Delta^2 = \frac{(1-a_2)\sigma_\varepsilon^2}{(1+a_2)\left[(1-a_2)^2 - a_1^2\right]} \tag{9}$$

Let κ_m be the autocorrelation in $\{\Delta_I(n)\}$ at lag m ($m > 0$). Then [2],

$$\kappa_m = \frac{A(1-B^2)A^m - B(1-A^2)B^m}{(A-B)(1+AB)} \tag{10}$$

where A and B are the roots of the characteristic equation $x^2 - a_1 x - a_2 = 0$. For all the traces, the fitting resulted in $a_1^2 + 4a_2 \geq 0$, so that the roots are always real. This means that κ_m is a mixture of damped exponentials.

Since $\{X_I^*(n)\}$ and $\{\Delta_I(n)\}$ are stationary and mutually independent, $\{X_I(n)\}$ is also a stationary process. The random variables $X_I(1), X_I(2), \ldots$, are identically distributed with common *pdf* f_{X_I} that is given by the convolution of $f_{\widetilde{X}_I}$ and f_Δ.

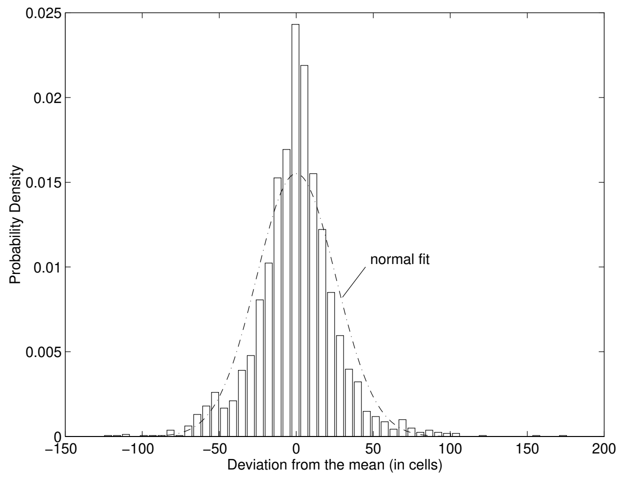

Figure 7: Probability distribution for $\{\widehat{\Delta}_I(n)\}$ (Oz trace).

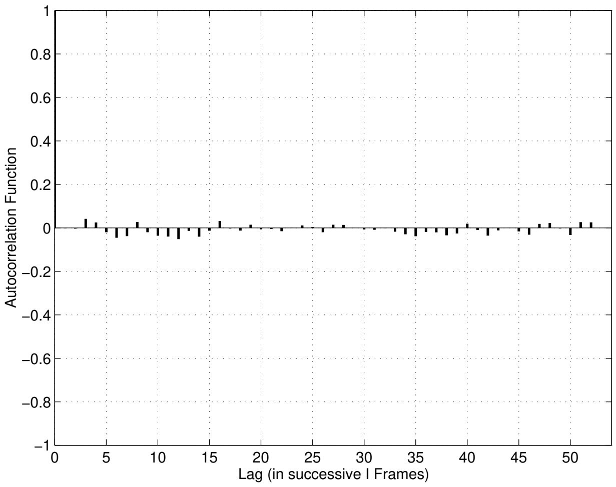

Figure 8: ACF of the empirical residuals in the AR(2) fit (Oz trace).

Proposition 2 *Let $\rho_I(m)$ be the ACF for $\{X_I(n)\}$ at lag m. Then,*

$$\rho_I(m) = \frac{q^m v_{\widetilde{X}_I} + \kappa_m \sigma_\Delta^2}{v_{\widetilde{X}_I} + \sigma_\Delta^2}. \tag{11}$$

Proof: For $m > 0$,

$$\begin{aligned}\rho_I(m) &\triangleq \frac{E\left[(X_I(1) - m_{X_I})(X_I(1+m) - m_{X_I})\right]}{v_{X_I}} \\ &= \frac{E\left[X_I^*(1)X_I^*(1+m)\right] + E\left[\Delta_I(1)\Delta_I(1+m)\right] - m_{X_I}^2}{v_{X_I}}\end{aligned} \tag{12}$$

(since $\{X_I^*(n)\}$ and $\{\Delta_I(n)\}$ are independent, and $E\left[\Delta_I(n)\right] = 0$). The variance of $X_I(1)$ is given by $v_{X_I} = v_{\widetilde{X}_I} + \sigma_\Delta^2$. Consider the numerator of the RHS of (12). The probability that the first I frame and the $(1+m)$th I frame belong to the same scene is q^m. Thus, $X_I^*(1) = X_I^*(1+m)$ with probability q^m. Otherwise, $X_I^*(1)$ and $X_I^*(1+m)$ are independent. Therefore,

$$E\left[X_I^*(1)X_I^*(1+m)\right] = \begin{cases} E\left[X_I^*(1)^2\right], & w.p. q^m \\ E\left[X_I^*(1)\right] E\left[X_I^*(m+1)\right], & w.p. (1-q^m) \end{cases}$$

Also, $E\left[\Delta_I(1)\Delta_I(1+m)\right] = \kappa_m \sigma_\Delta^2$. Thus, (12) becomes

$$\rho_I(m) = \frac{q^m E\left[X_I^*(1)^2\right] + (1-q^m)E^2\left[X_I^*(1)\right] + \kappa_m\sigma_\Delta^2 - m_{X_I}^2}{v_{\widetilde{X}_I} + \sigma_\Delta^2} \tag{13}$$

which reduces to (11) after some manipulations. □

From the above proposition, the ACF of $\{X_I(n)\}$ drops off at a rate that is determined by the sum of $q^m v_{\widetilde{X}_I}$ and $\kappa_m \sigma_\Delta^2$. The first term, which results from correlations due to scene effect, decreases at a geometric rate. The second term, which results from the autocorrelations in $\{\Delta_I(n)\}$, decreases as a sum of damped exponentials. Typically, the first term is dominant and $\rho_I(m)$ decreases approximately at a geometric rate. *Thus, the generating process for I frames is short-range dependent.* We will see later that when the three processes that generate I, P, and B frames are intermixed, the composite model exhibits long-range dependence.

3.2.2 P and B Frames

The sizes of P and B frames are modeled by two processes $\{X_P(n)\}$ and $\{X_B(n)\}$ of *i.i.d.* rvs and corresponding *pdf*s f_{X_P} and f_{X_B}, respectively. Although the empirical frame sizes for P frames (also B frames) are correlated, these correlations are negligible compared to the correlations between different types of frames (which are induced by the structure of the GOP pattern). In [12] we found that f_{X_P} and f_{X_B} can be appropriately characterized by lognormal distributions with parameters (μ_P, σ_P) and (μ_B, σ_B), respectively. In fact, a gamma or a Weibull *pdf* can also be used, with slightly less accurate fitting (see [12] for details).

Table 4 summarizes the fitting results for the four empirical traces. Estimates of the nine parameters that specify the model are provided. As expected, the estimated values vary from one trace to another. For parameters associated with the lognormal distributions, the estimates depend strongly on the dimensions of the captured frames. For the other parameters (a_1, a_2, and σ_ε), the estimates depend on the scene dynamics as well.

3.3 The Autocorrelation Structure

We now derive the ACF for the complete (composite) model. Let X_n be the size of the nth frame (which can be of any type) in the model. First, we need to check the stationarity of $\{X_n\}$. It is clear that if $\{X_n\}$ is generated such that the first frame is an I frame, the second a B, the third a B, and so on, then $\{X_n\}$ is nonstationary since the frame size distribution varies with n. However, if we start $\{X_n\}$ from an arbitrary frame location in the GOP pattern and from that point continue to generate frames according to the GOP pattern, then we can show that $\{X_n\}$ is stationary. This scenario is quite realistic considering that MPEG streams at an ATM multiplexer are admitted at different times. Thus, when the first frame (which is an I frame) of a newly admitted stream arrives at the multiplexer, the other ongoing streams could be sending other types of frames. From the perspective of the new stream, the ongoing streams look as if they were initialized at different locations of their GOP patterns.

Let S_n be a discrete random variable that describes the location of the nth frame within the GOP pattern. The state space for S_n is $\Omega_S = \{1, 2, \ldots, N\}$. S_n determines the frame type: if $S_n = 1$, then the type is I; if $S_n = 1+M,\ 1+2M, \ldots,\ 1+(N-M)$, then the type is P; otherwise, it is B. Given $S_n = i$, the distribution of X_n is stationary and depends only on i. For $i = 1, \ldots, N$, let $F_i(u) \triangleq \Pr\left[X_n \le u / S_n = i\right]$, and let $f_i(u)$ be the corresponding *pdf*. It is easy to see that $\{S_n\}$ is an irreducible homogeneous Markov chain with transition probabilities $p_{ij} \triangleq \Pr\left[S_n = j / S_{n-1} = i\right] = 1$ for $j = i+1$, $i = 1, \ldots, N-1$, and for $i = N$ and $j = 1$. Otherwise, $p_{ij} = 0$. All states of the chain are positive recurrent with mean recurrence time N. Thus, there is a unique stationary distribution Π such that $\Pi\mathcal{P} = \Pi$. Let $\Pi = [\pi_1\ \pi_2\ \ldots\ \pi_N]$. Then, $\pi_i = 1/\text{mean recurrence time } = 1/N$ for all i.

Proposition 3 *If $S_1 \sim \Pi$, then the process $\{X_n\}$ is strictly first-order stationary with marginal pdf:*

$$\begin{aligned} f_X(u) &= \frac{1}{N}\sum_{i=1}^{N} f_i(u) = \frac{1}{N}\left[f_{X_I}(u) + (N/M - 1)f_{X_P}(u)\right. \\ &\quad \left. + (N - N/M)f_{X_B}(u)\right]. \end{aligned} \tag{14}$$

Moreover, the mean and variance of X_n are given by:

$$m_X = \frac{1}{N}\left[m_{X_I} + (N/M - 1)m_{X_P} + (N - N/M)m_{X_B}\right]$$

$$\begin{aligned} v_X &= \frac{1}{N}\left[v_{X_I} + m_{X_I}^2 + (N/M - 1)(v_{X_P} + m_{X_P}^2)\right. \\ &\quad \left. + (N - N/M)(v_{X_B} + m_{X_B}^2)\right] - m_X^2. \end{aligned}$$

Proof: If $S_1 \sim \Pi$, then the Markov chain $\{S_n\}$ is stationary, i.e., $\Pr\left[S_k = i\right] = \pi_i = 1/N$ for all i and k.

$$\begin{aligned} \Pr\left[X_n \le u\right] &= \sum_{i=1}^{N} \Pr\left[X_n \le u / S_n = i\right] \Pr\left[S_n = i\right] \\ &= \frac{1}{N}\sum_{i=1}^{N} F_i(u). \end{aligned} \tag{15}$$

Taking the derivative of (15), we obtain (14), which shows that $\{X_n\}$ is first-order stationary. The expressions for the mean and variance follow in a straightforward manner. □

Trace	$\widetilde{\mu}_I$	$\widetilde{\sigma}_I$	a_1	a_2	σ_ε	μ_P	σ_P	μ_B	σ_B
Oz	5.9651	0.4832	0.5300	0.1512	19.8	4.8294	0.6443	3.9039	0.2746
Star Wars	4.9147	0.3861	0.2088	0.0917	8.9644	3.9324	0.5843	2.8049	0.5242
Lambs	4.5813	0.3852	0.3965	0.1516	4.36	2.5884	0.8721	1.9861	0.6937
Bond	5.3050	0.3663	0.4271	0.0380	10.3	4.5656	0.5111	3.2572	0.3761

Table 4: Estimates of the various parameters used in the model. MLE are used for $\widetilde{\mu}_I$, $\widetilde{\sigma}_I$, μ_P, σ_P, μ_B, and σ_B. Yule-Walker estimates are used for a_1 and a_2. σ_ε^2 is estimated by the sum-of-squares of the residuals divided by the number of I frames.

It can be further shown that $\{X_n\}$ is also strictly second-order stationary. We skip the proof and proceed to provide the ACF for $\{X_n\}$.

Proposition 4 *Let ρ_k be the ACF for $\{X_n\}$ at lag k, and let $h(i,k) \triangleq [(i+k-1) \bmod N]+1$. Then,*

$$\rho_k = \frac{1}{Nv_X}\sum_{i=1}^{N}\{E[X_1/S_1=i]\,E[X_1/S_1=h(i,k)]\} - m_X^2/v_X \qquad (16)$$

for all $k \neq N,\ 2N, \ldots$, and

$$\rho_k = \frac{1}{Nv_X}\left\{\sum_{i=2}^{N}E^2[X_1/S_1=i] + (1/N)E[X_1X_{1+k}/S_1=1]\right\} - m_X^2/v_X \qquad (17)$$

for $k = N,\ 2N, \ldots$.

Proof: see appendix. □

All the quantities in the RHS of (16) and (17) are known. The middle term in (17) reflects the contribution of the correlations between I frames only, and is given by:

$$E[X_1X_{1+k}/S_1=1] = q^m E\left[(X_I^*)^2\right] + (1-q^m)E^2[X_I^*] + \kappa_m\sigma_\Delta^2 \qquad (18)$$

where $m = k/N$. The following remarks can be made about the ACF in (16) and (17). First, at lags that are not multiples of N, the first term in (16) can take only two possible values: one value when $k-1$ is a multiple of M (i.e., $k = M+1,\ 2M+1, \ldots$), and another value for all other k, $k \neq$ multiple of N. Second, at lags which are multiples of N, the middle term in (17), which is given in (18), decreases almost exponentially with k to its asymptotic limit $(1/N)E^2[X_I^*] = (1/N)E^2[X_1/S_1=1]$. The other two terms in the numerator do not change with k. Thus, as k goes to infinity at increments of N, ρ_k converges to a positive value given by:

$$\lim_{k\to\infty}\rho_{kN} = \frac{\frac{1}{N}\sum_{i=1}^{N}E^2[X_1/S_1=i] - m_X^2}{v_X} \qquad (19)$$

Although the ACF for $\{X_I(n)\}$ decreases exponentially, the ACF for the composite sequence $\{X_n\}$ does not converge to zero. The nonzero limit is the consequence of the cross-correlations between different types of frames, which are *induced* by periodically generating frames according to the GOP pattern. Thus, although $\{X_I(n)\}$ is Markovian (exhibits short-range dependence), and $\{X_P(n)\}$ and $\{X_B(n)\}$ are *i.i.d.* sequences, the *composite model* exhibits long-range dependence since $\sum_{k=0}^{\infty}\rho_k = +\infty$. Enhancing the model by incorporating the autocorrelations in $\{X_P(n)\}$ and $\{X_B(n)\}$ will have minor impact on the overall correlation structure. It should be noted that the typically discussed form of LRD where the ACF has the form $k^{-\beta}$ [1] is only one special case of LRD which, according to Cox's definition [3], includes all second-order stationary processes with non-summable ACF.

4 Generating Synthetic MPEG Streams

The algorithm in Figure 9 can be used to generate synthetic MPEG streams based on the proposed model.

```
set Scene_max := desired number of scenes
X ≜ frame size (in cells)

 for j = 1 to Scene_max do
    generate scene length: N_j ~ Geometric(p)
    generate X̃_I(j) ~ lognormal(μ̃_I, σ̃_I)
    for i = 1 to N_j do
       for k = 1 to N do
          if k = 1, then          /* I frame */
             X = X̃_I(j) + Δ_I(i), where
             Δ_I(i) = â_1 Δ_I(i − 1) + â_2 Δ_I(i − 2) + ε(i)
          else
             if remainder(k/M) = 1, then /* P frame */
                X ~ lognormal(μ̂_P, σ̂_P)
             else                 /* B frame */
                X ~ lognormal(μ̂_B, σ̂_B)
             end if
          end if
       end for
    end for
end for
```

Figure 9: Algorithm for generating a synthetic video stream.

An example of a synthetic stream based on the fitting of *Oz* trace is shown in Figure 10. The analytical ACF of the model is plotted in Figure 11. Comparing these figures to their counterparts in the real data, we observe that the model captures the general shapes of the frame size distribution and ACF of an MPEG stream. However, correlation values in the model are slightly less than the empirical ACF, mainly because of our simplifying assumptions regarding the correlations in each of the three subsequences. Nevertheless, the model captures the induced correlations that result from the periodicity of the GOP pattern and the large differences in the sizes of different types of frames, and these correlations seem to have the major impact on the overall correlation structure.

5 Queueing Performance at an ATM Multiplexer

Traffic models are commonly used to predict the queueing performance at a statistical multiplexer. Therefore, the appropriateness of a model is ultimately determined by its ability to accurately predict the actual queueing behavior. To

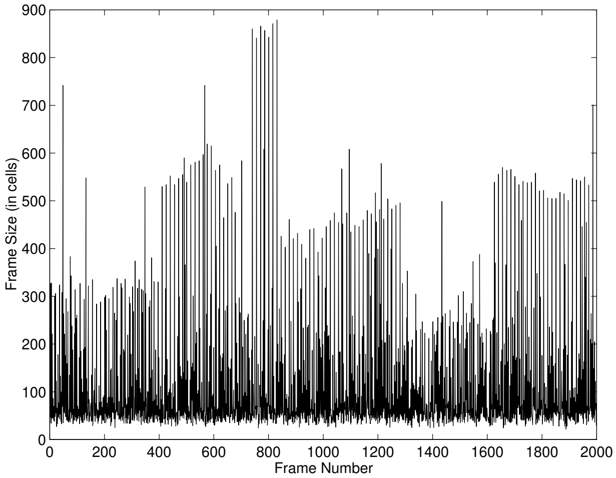

Figure 10: Example of a synthetic trace.

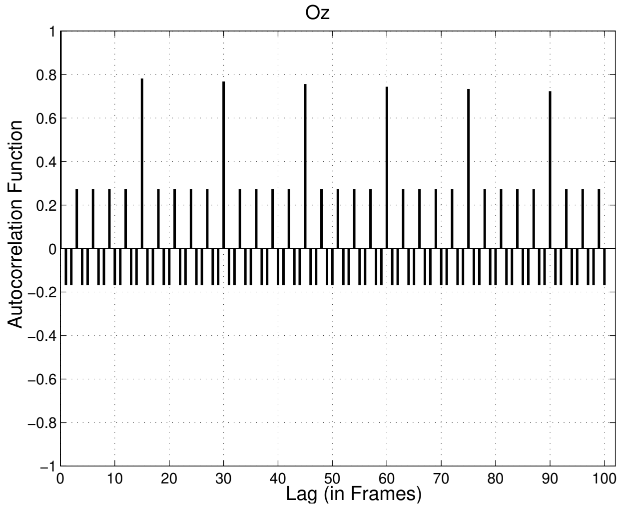

Figure 11: ACF for the frame-size sequence based on model.

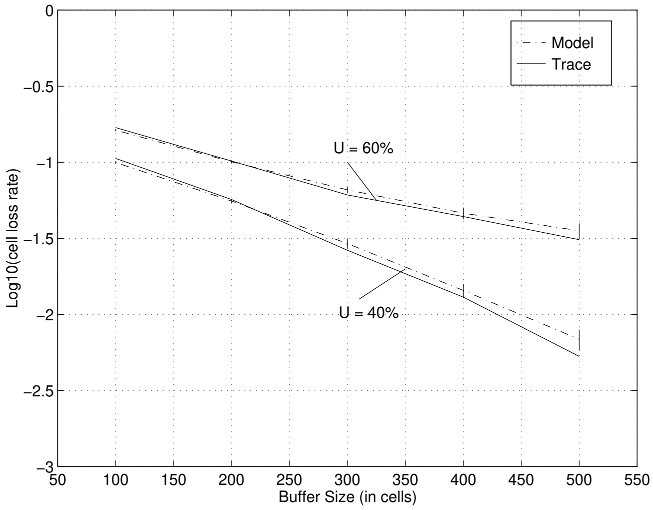

Figure 12: Cell loss rate versus buffer size for one stream.

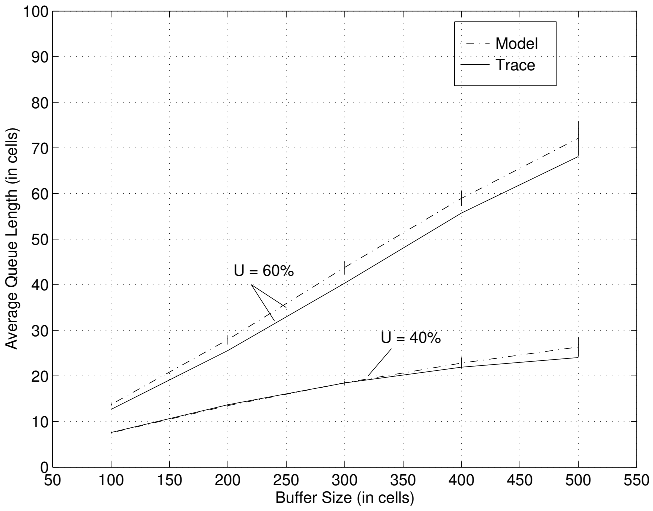

Figure 13: Average queue length versus buffer size for one stream.

examine the goodness of our model, we conduct simulation experiments of a finite FIFO queue whose input consists of real traces as well as synthetic traces generated according to the model. Our primary measure of interest is the cell loss rate. Due to space limitations, only the results for *Oz* trace and its synthetic counterparts are reported.

First, we examine the queueing performance for a single stream (i.e., no multiplexing). Figures 12 and 13 depict the cell loss rate and the average queue length, respectively, at two loads: $U = 40\%$ and $U = 60\%$. Twenty simulation replications are used to obtain the model-related results (the 95% confidence intervals are indicated by the short vertical lines). For small buffers, the model predictions are very accurate. As buffer size increases, the model starts to slightly overestimate the loss rate. We attribute this behavior to the persistent correlations in the model (Proposition 4). For practical buffer sizes, the discrepancy is small. Note that even at a light load of 40%, the cell loss rate (both actual and predicted) under a single video stream is quite high. This is a consequence of the bursty and correlated nature of MPEG video traffic. To obtain smaller loss rates, the buffer size must be significantly increased or the load must be reduced. Unfortunately, the empirical traces are not long enough to give statistically credible results at very small loss rates, say below 10^{-4}. The reason is that a cell loss rate of 10^{-4} implies the loss of a few hundreds of cells from a given empirical trace (e.g., 716 cells in *Star Wars*). Cell losses are strongly correlated as they mainly occur in few (sometimes less than ten) large I frames of a given trace. Because of the strong correlations between successive I frames within a scene, the errorred frames are also correlated, so the few hundreds of lost cells come from a handful of scenes. Longer video traces are needed to investigate very low loss rates for a single stream. At loads above 60%, the loss rate is very high, and the model predictions are expectedly very accurate (not shown here).

Next, we examine the loss performance for multiplexed video streams. One difficulty in doing such a study is that the loss performance for multiplexed MPEG sources with I, P, and B frames strongly depends on the manner in which the GOP periods of different sources are aligned. For example, if we multiplex two sources that have the same GOP pattern, then the highest loss rate is observed when I frames from both sources arrive simultaneously at the multiplexer. Because of the periodicity of the GOP pattern, I frames from the two sources continue to overlap, causing large cell losses. On the other hand, if an I frame from the first source and a B frame from the other source (say the first B frame in the GOP) overlap in time, the loss rate is reduced by several orders of magnitude. This means that the cell loss rates from several simulations of *arbitrarily arranged* multiplexed MPEG streams cannot be regarded as *i.i.d.* random variables, and thus confidence intervals cannot be constructed. It is more appropriate to study the loss performance under a particular "arrangement" of the multiplexed streams. The impact of arranging MPEG streams on the allocation of bandwidth was studied in [13] within a deterministic framework. Since our interest here is in evaluating the model's accuracy rather than studying the effect of stream scheduling, we limit our simulation experiments (for both real and synthetic data) to the "optimal" arrangement of that was shown in [13] to give the minimum effective bandwidth. According to this optimal arrangement, the multiplexed streams are aligned such that a GOP of the first source is one frame lag from a GOP of the second source, a GOP of the second source is one frame lag from a GOP of the third source, and so on. Frame boundaries are aligned. An example of the temporal structure for optimally arranged five sources with common GOP pattern *IBBPBB* is shown in Figure 14.

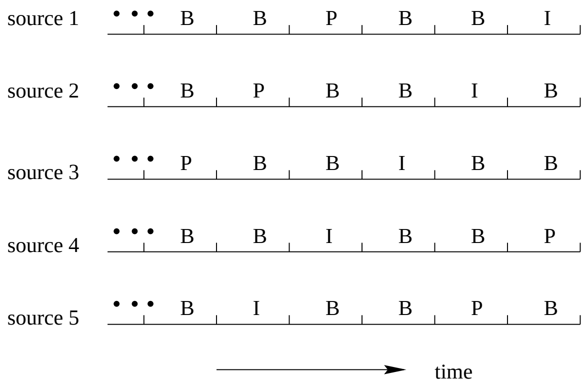

Figure 14: Example of the "optimal" arrangement of multiplexed MPEG streams with GOP pattern *IBBPBB*.

Table 5 depicts the cell loss performance for five multiplexed streams using real and synthetic data. Streams are aligned "optimally" as shown in Figure 14. To produce fives real sources from *Oz* trace, we used a commonly employed approach in which the empirical trace is arranged as a circular list. A real source starts at some frame location in the list and continues until it completes the circle. One problem with this approach is that the extracted streams are not exactly independent, especially when their starting frames are not far apart. Unfortunately, no other alternative is available if multiplexing of structurally similar real sources is to be studied. To reduce the possibility of correlations between different sources, we select the starting times of different sources to be as far as possible from each other (typically, the starting frames are chosen randomly [7]). The loss rates for the synthetic streams in Table 5 are averaged over ten independent simulation replications. Sample variances of the loss rates for the synthetic data ranged from 1% to 10% of the mean values. Hence, the confidence intervals are sufficiently tight (they are not shown for brevity). From the table, it is observed that the model provides sufficiently good predictions of the queueing performance. The model, however, slightly underestimates the loss rate at small buffer sizes. As the buffer size increases, the gap is reduced and eventually the model starts to overestimate the performance. For practical buffer sizes, the model's predictions are quite acceptable.

Given the demonstrated appropriateness of the model, it can be used to study the multiplexing of large number of streams and determine the required amounts of resources to guarantee a desired level of loss performance. In this case, the model offers the means to generate statistically similar but independent sources. We present some simulation examples that show the practical use of the model. Figure 15 depicts the cell loss rate versus buffer size for 10 multiplexed video streams at three loads. Each simulation experiment was repeated 10 times, each time with 10 different synthetic sequences (95% confidence intervals are indicated by the short vertical lines). Each synthetic stream consisted of 200,000 frames. With this number of frames, statistically credible results can be obtained for very small loss rates. Figure 16 depicts the cell loss rate versus the number of multiplexed streams at a given load and buffer size (W). The results are averaged over ten independent replications (confidence intervals are sufficiently tight, and are not shown for brevity). In general, increasing the number of multiplexed streams while fixing the load and the buffer size results in a smaller loss rate, with the effect being more pronounced at lighter loads (notice that buffer size is not normalized to the number of streams). However, this trend is not always true. In particular, a sudden increase in the loss rate is observed when the number of multiplexed streams goes from 15 to 16. This increase is related to the manner in which the streams were arranged. According to the "optimal" arrangement, I frames of a given source are one frame period apart from I frames of the subsequent source. With a GOP period of 15 frames ($N = 15$ for *Oz* sources), a maximum of 15 sources can be arranged without overlapping I frames of different sources. After that, the overlap is inevitable, causing the observed increase in the loss rate when 16 sources are multiplexed. Some less obvious effects due to the overlap of P frames can also be noticed. A more elaborate study of the impact of stream alignment on the loss rate will be provided in a future paper.

6 Summary

We presented a comprehensive traffic model for MPEG-coded video streams with all types of MPEG frames. The model was successfully fitted to four different empirical video sequences. In addition to approximating the marginal distributions for frame sizes and the overall correlation structure, the model uses a scene-related component to capture bit rate variations at multiple time scales. We found that the fluctuations of I frames can be characterized by a modulated process in which the local variations are modeled by an AR(2) process that varies around a scene-related random mean. Two autocorrelated processes were needed to characterize I frames. The sizes of P and B frames were modeled by two *i.i.d.* random processes with lognormal marginals. We derive the analytical form for the autocorrelation function for the composite model. This form indicates the existence of persistent correlations that are attributed to the periodicity of the GOP pattern and the significant differences between the sizes of different types of frames. The sum of these correlations (over all lags) is infinite. Thus, although the individual random subsequences are Markovian,

Buffer Size (in cells)	$U = 80\%$		$U = 70\%$		$U = 60\%$	
	Real	Model	Real	Model	Real	Model
100	9.92E−2	6.72E−2	6.04E−2	3.85E−2	2.53E−2	1.70E−2
200	8.10E−2	5.08E−2	4.32E−2	2.60E−2	1.37E−2	9.51E−3
300	6.56E−2	3.89E−2	3.05E−2	1.74E−2	7.34E−3	4.98E−3
400	5.18E−2	2.97E−2	2.12E−2	1.15E−2	3.98E−3	2.61E−3
500	3.97E−2	2.24E−2	1.41E−2	7.55E−3	2.13E−3	1.37E−3
600	2.95E−2	1.67E−2	9.09E−3	4.93E−3	1.06E−3	7.04E−4
700	2.12E−2	1.23E−2	5.76E−3	3.17E−3	4.56E−4	3.56E−4
800	1.49E−2	8.84E−3	3.53E−3	1.99E−3	1.42E−4	1.73E−4

Table 5: Cell loss rate when five streams are multiplexed.

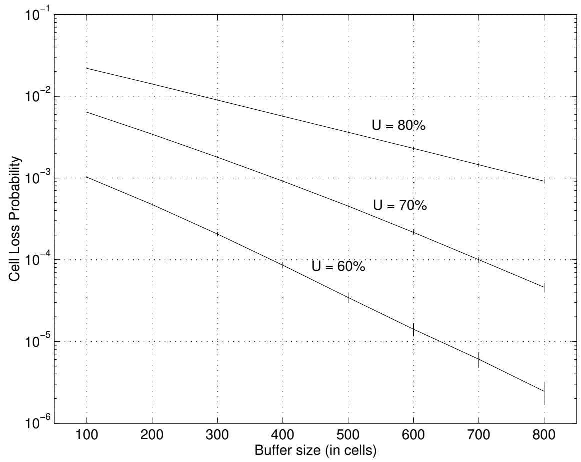

Figure 15: Cell loss rate for ten multiplexed streams based on the model.

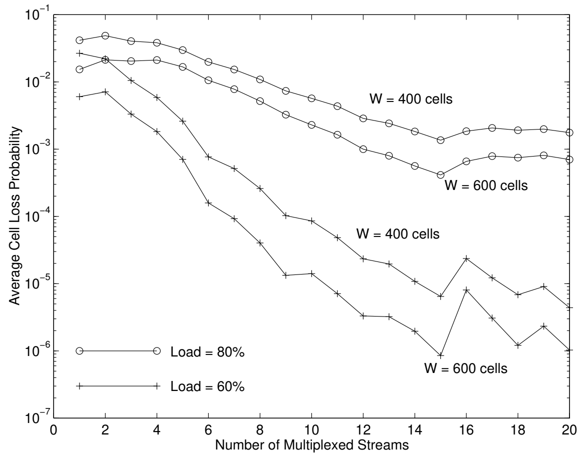

Figure 16: Cell loss rate versus the number of multiplexed streams (based on model)

the mixing according to a fixed GOP pattern renders the model long-range dependent. This, somehow surprising, result can be extended to stationary processes with different marginals that are intermixed according to a fixed periodic pattern. Simulations were used to show the appropriateness of the model in predicting the queueing performance for real video sources. Model-based synthetic streams were used to study the performance of multiplexed MPEG streams. For such studies, the model provides a much easier and less expensive approach to generating synthetic traces than having to obtain real ones.

Acknowledgment

The authors would like to thank Mark Garrett and Oliver Rose for making their MPEG traces available. They also thank the anonymous referees for their helpful comments.

Appendix
Proof of Proposition 4

To show that the ACF for $\{X_n\}$ is given by (16) and (17), we consider two cases:

Case 1: $k \neq N,\ 2N, \ldots$

$$\rho_k \triangleq \frac{E\left[(X_1 - m_X)(X_{1+k} - m_X)\right]}{v_X} \tag{20}$$

$$= \frac{E\left[X_1 X_{1+k}\right] - m_X^2}{v_X} \tag{21}$$

Consider the term $E\left[X_1 X_{1+k}\right]$.

$$E\left[X_1 X_{1+k}\right] = \int_0^\infty \Pr\left[X_1 X_{1+k} > u\right] du$$

$$= \int_0^\infty \sum_{i=1}^{N} \Pr\left[X_1 X_{1+k} > u / S_1 = i\right] \cdot \Pr\left[S_1 = i\right] du$$

$$= \sum_{i=1}^{N} \pi_i E\left[X_1 X_{1+k} / S_1 = i\right] = \frac{1}{N} \sum_{i=1}^{N} E\left[X_1 X_{1+k} / S_1 = i\right]$$

The two events $[X_1 \leq x_1 / S_1 = i]$ and $[X_{1+k} \leq x_2 / S_1 = i]$ are (conditionally) independent for $k \neq$ multiple of N. Thus,

$$E\left[X_1 X_{1+k}\right] = \frac{1}{N} \sum_{i=1}^{N} E\left[X_1 / S_1 = i\right] E\left[X_{1+k} / S_1 = i\right]$$

$$= \frac{1}{N}\sum_{i=1}^{N} E\left[X_1/S_1 = i\right] E\left[X_{1+k}/S_{1+k} = h(i,k)\right]$$
$$= \frac{1}{N}\sum_{i=1}^{N} E\left[X_1/S_1 = i\right] E\left[X_1/S_1 = h(i,k)\right]$$

Case 2: $k = N, 2N, \ldots$.
In this case, $E\left[X_1 X_{1+k}\right]$ can be written as

$$\frac{1}{N}\sum_{i=2}^{N} E\left[X_1 X_{1+k}/S_1 = i\right] + \frac{1}{N} E\left[X_1 X_{1+k}/S_1 = 1\right]$$

For $i = 2, 3, \ldots, N$, $E\left[X_1 X_{1+k}/S_1 = i\right] =$

$$E\left[X_1/S_1 = i\right] E\left[X_{1+k}/S_1 = i\right] = E^2\left[X_1/S_1 = i\right]$$

(the first equality holds because each of the subsequences $\{X_P(n)\}$ and $\{X_B(n)\}$ are *i.i.d.*. The second equality holds because, in this case, $S(1+k) = S(1+mN) = S(1)$). The term $E\left[X_1 X_{1+k}/S_1 = 1\right] = E\left[X_I(1) X_I(1+m)\right]$ which is given in the proof of Proposition 2. $\square$

References

[1] J. Beran, R. Sherman, M. S. Taqqu, and W. Willinger. Long-range dependence in variable bit-rate video traffic. *IEEE Transaction on Communications*, 43:1566–1579, 1995.

[2] G. E. P. Box and G. M. Jenkins. *Time Series Analysis: Forcasting and Control.* Holden-Day, Inc., 1976. (Revised Edition).

[3] D. R. Cox. Long-range dependence: A review. In H. A. David and H. T. David, editors, *Statistics: An Appraisal*, pages 55–74. The Iowa State University Press, Ames, Iowa, 1984.

[4] M. R. Frater, J. F. Arnold, and P. Tan. A new statistical model for traffic generated by VBR coders for television on the Broadband ISDN. *IEEE Trans. on Circuits and Systems for Video Technology*, 4(6):521–526, Dec. 1994.

[5] M. W. Garrett and W. Willinger. Analysis, modeling, and generation of self-similar VBR video traffic. In *Proceedings of the SIGCOMM'94 Conference (Computer Communications Review)*, pages 269–280, Sept. 1994.

[6] D. Heyman, E. Tabatabai, and T. Lakshman. Statistical analysis of MPEG2-coded VBR video traffic. In *Proc. of the Sixth International Workshop on Packet Video*, 1994.

[7] D. P. Heyman, A. Tabatabai, and T. V. Lakshman. Statistical analysis and simulation study of video teleconferencing traffic in ATM networks. *IEEE Trans. on Circuits and Systems for Video Technology*, 2(1):49–59, Mar. 1992.

[8] C. Huang, M. Devetsikiotis, I. Lambadaris, and A. Kaye. Modeling and simulation of self-similar variable bit rate compressed video: A unified approach. In *Proc. of SIGCOMM '95*, 1995.

[9] B. Jabbari, F. Yegengolu, Y. Kuo, S. Zafar, and Y.-Q. Zhang. Statistical characterization and block-based modeling of motion-adaptive coded video. *IEEE Trans. on Circuits and Systems for Video Technology*, 3(3):199–207, June 1993.

[10] P. A. Jacobs and P. A. W. Lewis. Time series generated by mixtures. *Journal of Time Series Analysis*, 4(1):19–36, 1983.

[11] M. Krunz and H. Hughes. A traffic model for MPEG-coded VBR streams. In *Proc. of the ACM SIGMETRICS/PERFORMANCE '95 Conference*, pages 47–55, May 1995.

[12] M. Krunz, R. Sass, and H. Hughes. Statistical characteristics and multiplexing of MPEG streams. In *Proc. of the IEEE INFOCOM '95 Conference*, pages 455–462, Boston, Apr. 1995.

[13] M. Krunz and S. K. Tripathi. Impact of video scheduling on bandwidth allocation for multiplexed MPEG streams. *Multimedia Systems Journal*, 1996. (to appear).

[14] A. M. Law and W. D. Kelton. *Simulation Modeling and Analysis.* McGraw-Hill, Inc., second edition, 1991.

[15] A. A. Lazar, G. Pacifici, and D. E. Pendarakis. Modeling video sources for real-time scheduling. In *Proc. of IEEE GLOBECOM '93*, volume 2, pages 835–839, 1993.

[16] P. Pancha and M. El Zarki. Bandwidth-allocation schemes for variable-bit-rate MPEG sources in ATM networks. *IEEE Trans. on Circuits and Systems for Video Technology*, 3(3):190–198, June 1993.

[17] D. Reininger, B. Melamed, and D. Raychaudhuri. Variable bit rate MPEG video: Characteristics, modeling and multiplexing. In *Proc. of the 14th Int. Teletraffic Congress*, pages 295–306, Antibes Juan-les-Pins, France, June 1994.

[18] O. Rose. Statistical properties of MPEG video traffic and their impact on traffic modeling in ATM systems. In *Proceedings of the 20th Annual Conference on Local Computer Networks*, Minneapolis, MN, 1995.

[19] F. Yegengolu, B. Jabbari, and Y.-Q. Zhang. Motion-classified autoregressive modeling of variable bit rate video. *IEEE Trans. on Circuits and Systems for Video Technology*, 3(2):42–53, Feb. 1993.